



# Modeling Thermo-electrochemistry, Capacity Degradation, and Mechanics with SEI Layer

**Prof. Ann Marie Sastry, PI**

**Project ID: ES082**

Arthur F. Thurnau Professor, Mechanical, Biomedical and Materials Science and Engineering  
University of Michigan  
Ann Arbor, MI 48109-2125

**CONTRIBUTORS: Dr. Jonghyun Park, Dr. Jeong Hun Seo,  
Dr. Amit Gupta, Prof. Wei Shyy, Mr. Min Zhu**

*2011 DOE Annual Merit Review Meeting  
Arlington | May 11, 2011*

*This presentation does not contain any proprietary or confidential information*

**Advanced Materials Systems Laboratory**

Departments of Mechanical, Biomedical and Materials Science and Engineering



# acknowledgements

*Advanced Materials Systems Laboratory*

## sponsor

*DOE*

## Sastry group members

*Dr. Joseph Gallegos*

*Dr. Sangmin Lee*

*Mr. Yoon Koo Lee*

*Dr. Greg Less*

*Mr. Sang Woo Han*

*Mr. Dong Hoon Song*

*Mr. Ho Sop Shin*

## leverage

*General Motors*

*Oak Ridge National Laboratory*





# timeline and budget

A • M • S • L

## timeline

- project start date: Jan. 2010
- project end date: Apr. 2011
- percent complete: 90%

## budget

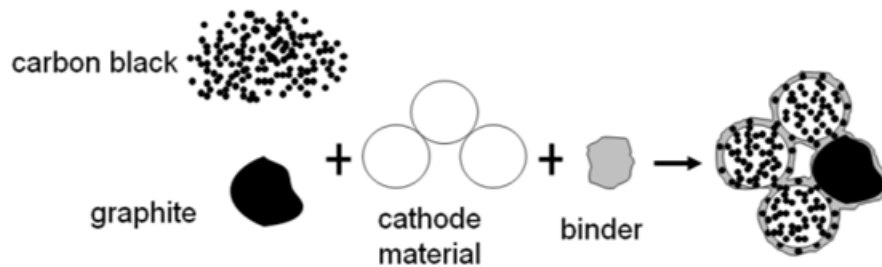
- total project funding
  - DOE share: \$ 320 K
- funding received in FY10
  - \$ 320 K
- funding for FY11
  - N/A

# barriers

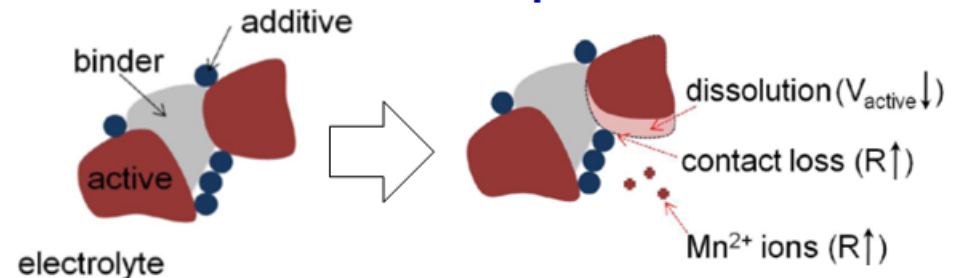
A • M • S • L

**BARRIERS:** short lithium battery lifetimes—capacity degradation, closely related to composition of electrode, particle aggregates and dissolution of particles; closely related to SEI layer formation on electrodes

electrode configuration (e.g., composition)

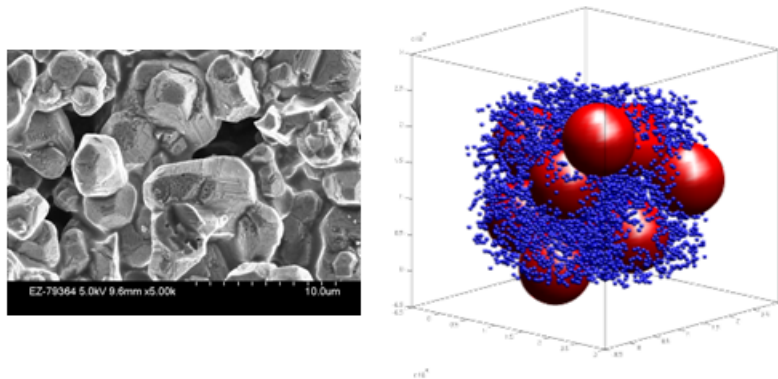


dissolution of active material particles

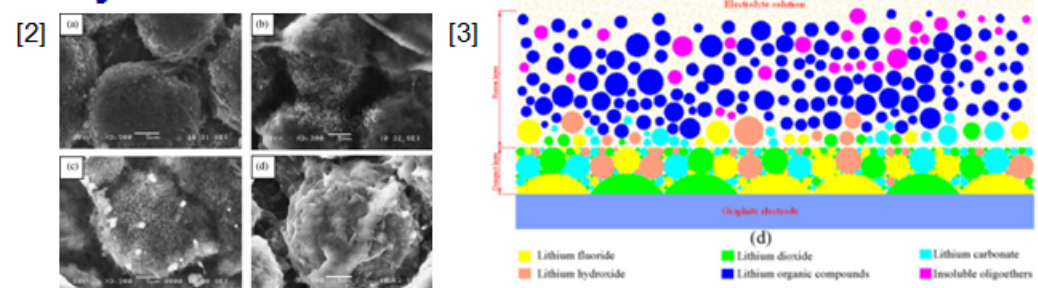


[1] J. Park, J.H. Seo, G. Plett, W. Lu and A.M. Sastry, "Numerical simulation of the effect of the dissolution of  $\text{LiMn}_2\text{O}_4$  particles on Li-ion battery performance," *Electrochem. Solid-State Lett.*, v. 14 (2), pp. A14-A18, 2011

particle aggregates  
(active material & additives)



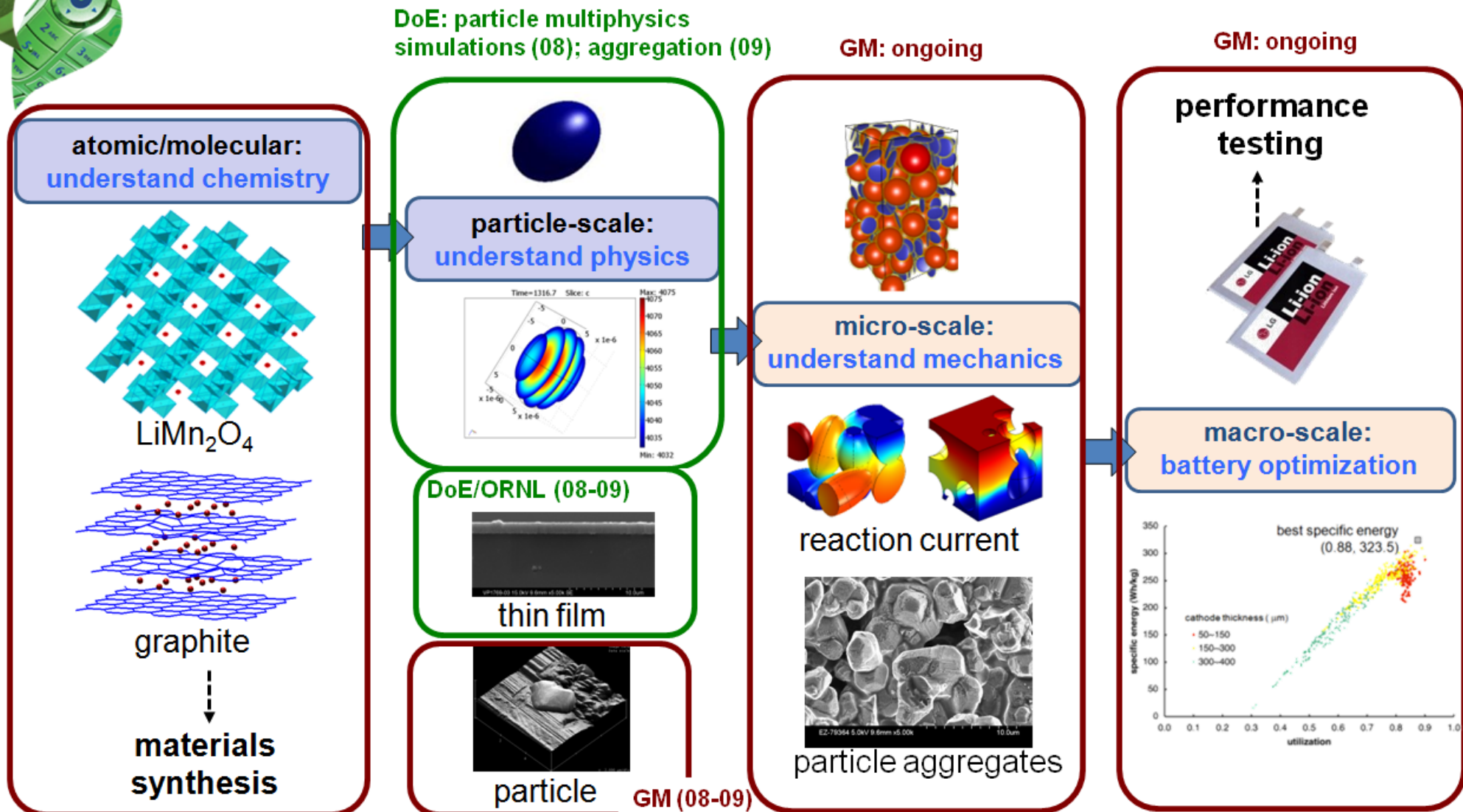
SEI layer formation



[2] P.L. Moss, G. Au, E.J. Plichta and J.P. Zheng, "Investigation of solid electrolyte interfacial layer development during continuous cycling using ac impedance spectra and micro-structural analysis," *Journal of Power Sources*, v. 189 (1), 2009

[3] J. Yana, B.-J. Xia, Y.-C. Su, X.-Z. Zhou, J. Zhang, X.-G. Zhang, "Phenomenologically modeling the formation and evolution of the solid electrolyte interface on the graphite electrode for lithium-ion batteries," *Electrochimica Acta*, v. 53, pp.7069-7078, 2008







# purpose of work

A • M • S • L

## OBJECTIVES:

Determine battery performance for high-power systems via multiscale FE modeling considering self-assembly, and the effect in turn on cathode dissolution as the main effect in capacity degradation. Investigate SEI layer formation mechanism. Validate SEI layer formation model through *ex situ* experimental techniques.

## MILESTONES:

- (a) implement multiscale modeling with self-assembly and dissolution (Mar. 11) (implemented)
- (b) implement modeling and simulation for multiple nucleation formation (May 11)
- (c) characterize microstructure, chemical elements of SEI layers, and impedance change due to SEI layers (Aug. 11)



# dissolution of active particles: FY10 A • M • S • L

## objectives

- derive volume fraction changes in electrodes due to dissolution and extend the porous electrode theory to correlate dissolution with capacity fade in Li-ion batteries
- map the nature of the effects of dissolution on the capacity decrease during cycling with different conditions, including temperature and voltage range

## approach

- calculate volume loss due to dissolution using shrinking unreacted-core model
- simulate 1D thermal-electrochemical model for battery performance
- study capacity fade and resistance change by changing temperature, voltage range, and cycle number

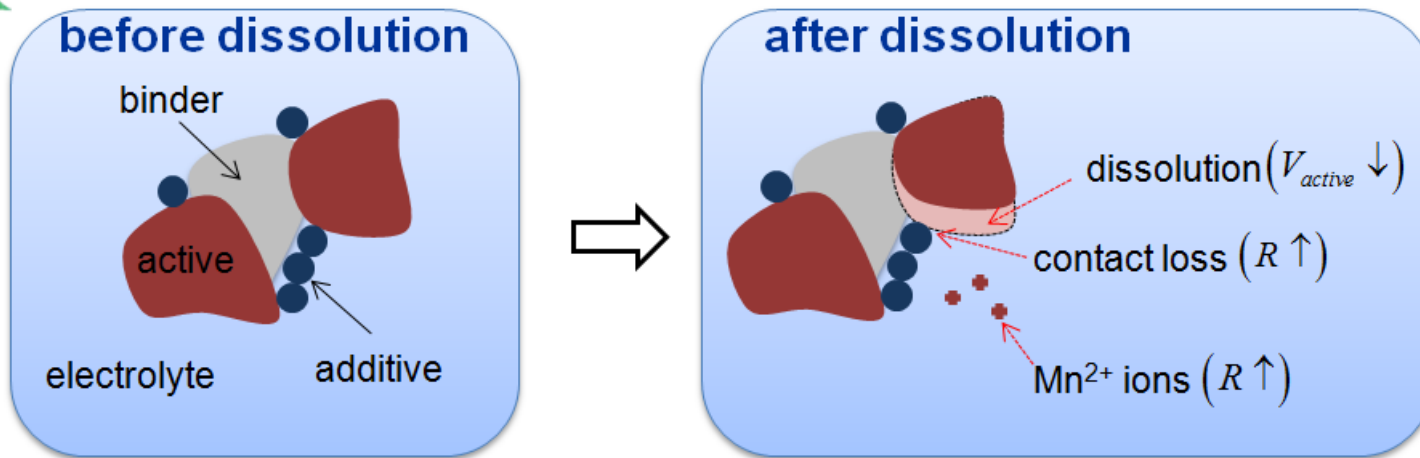
## finding/results

- a quantitative relationship between the volume fraction change due to dissolution and capacity fade
- material loss of active particles results in decreased effective transport properties in the solid phase, which in turn results in a reduction in electrochemical reaction rate, reducing capacity

## publications

- Park, J., Seo, J.H., Plett, G., Lu, W. and Sastry, A.M., "Numerical simulation of the effect of the dissolution of  $\text{LiMn}_2\text{O}_4$  particles on Li-ion battery performance", *Electrochemical and Solid-State Letters*, v. 14 (2), pp. A14-A18, 2011

# dissolution of active particles: FY10 A • M • S • L



## three main factors determining dissolution rate

- particle size: contact surface area
- temperature: reaction rate
- operating voltage: phase transition

## main dissolution effects on battery performance

- active material loss leads to direct capacity loss
- loss decreases the effective transport properties, resulting in a reduction of the electrochemical reaction rate, reducing capacity
- contact resistance increases due to the intimate contact loss between active and conductive particles
- the dissolved Mn<sup>2+</sup> ions transported, deposited on the anode side; deplete the anode by the reduction of Mn





# dissolution of active particles: FY10 A • M • S • L

## properties

### battery system

anode	graphite (100 $\mu\text{m}$ )
cathode	manganese oxide (183 $\mu\text{m}$ )
electrolyte	1M LiPF <sub>6</sub> in EC:DMC

### dissolving rate

particle	19.9 $\mu\text{m}$ in diameter (cathode) [1]
$E_a^*$	72.84 kJ/mol [1]
$K_0^*$	$3.41 \times 10^5 \text{ s}^{-1}$ [1]
$\omega^{**}$	2.8 times [3]

\* k is expressed by Arrhenius representation

$$k = k_0 \exp(-E_a / RT)$$

\*\* elevated reaction rate above 4.1 V and below 3.1 V

### AAS measurement

- dissolution ratio and reaction time [1, 2]
- $[1 - (1 - X_a)^{1/3}] = kt$
- $X_a$ : the dissolution reaction

### volume loss estimation

$$\bullet \frac{M_d^{3+}}{M_i^{3+}} = \frac{X_a}{1 + X_a}, M_d^{4+} = \frac{1}{2} M_d^{3+}$$

$$\bullet V = V_0 \left( 1 - \frac{0.304}{2} \frac{X_a}{X_a + 4} \right)$$

$i$ : initial,  $d$ : dissolved molar mass

### thermal-electrochemical model

- galvanostatic charge/discharge simulations with a limited voltage range

[1] C.-H. Lu and S.-W. Lin, *J. Mater. Res.*, **17**, 1476 (2002)

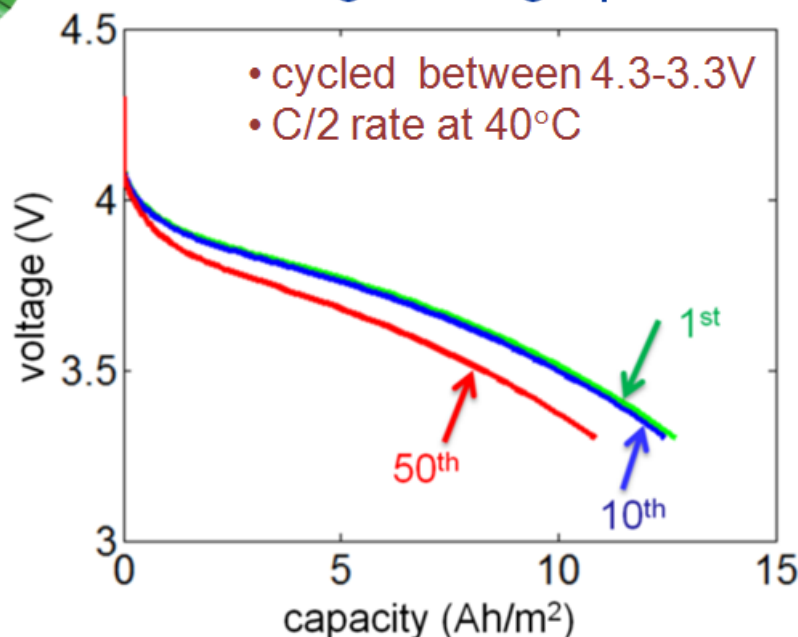
[2] O. Levenspiel, *Chemical Reaction Engineering*, John Wiley & Sons, New York (1972)

[3] Y. Xia, Y. Zhou, and M. Yoshio, *J. Electrochem. Soc.*, **144**, 2593 (1997)

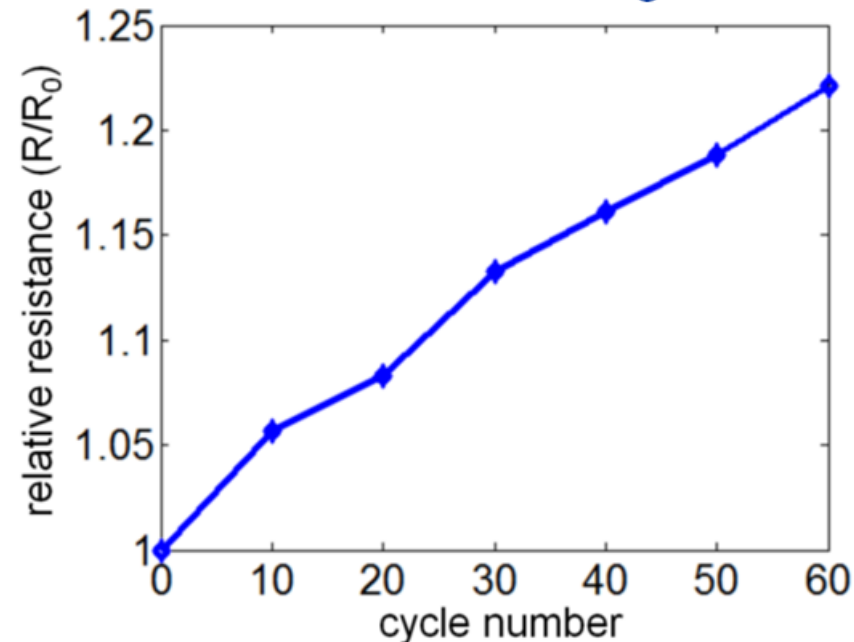


# dissolution of active particles: FY10 A • M • S • L

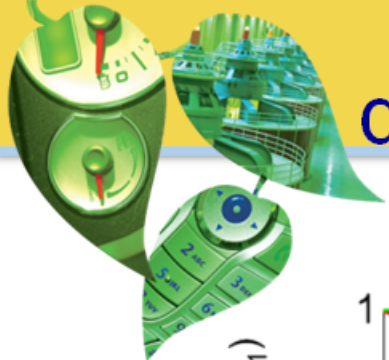
discharge voltage profile



resistance change

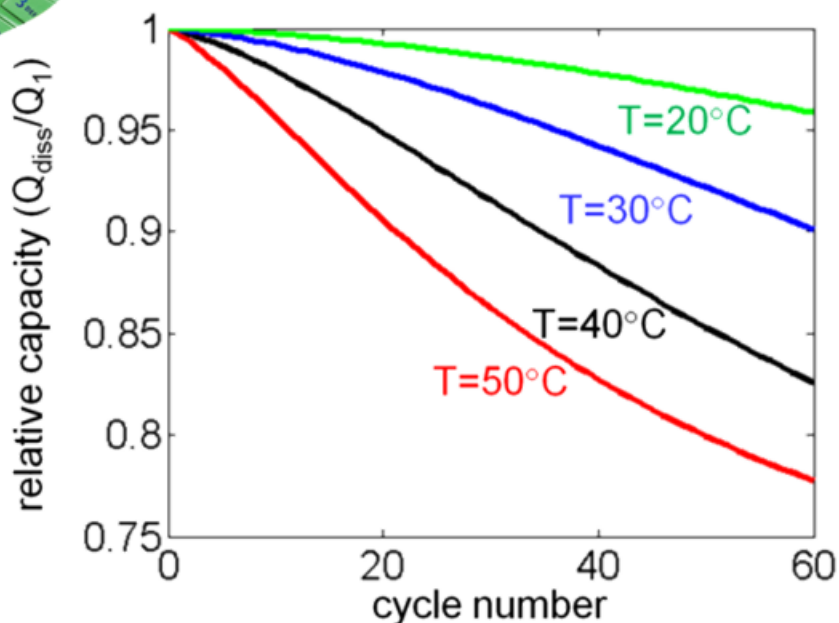


- after 50 cycles, the capacity decreases by 15% due to dissolution of the active particles
- the active material loss causes a delay in the reaction rate for insertion and deinsertion at the solid and electrolyte phase boundary, which results in an increase in resistance; the increase in resistance will cause a high polarization, resulting in apparent capacity losses

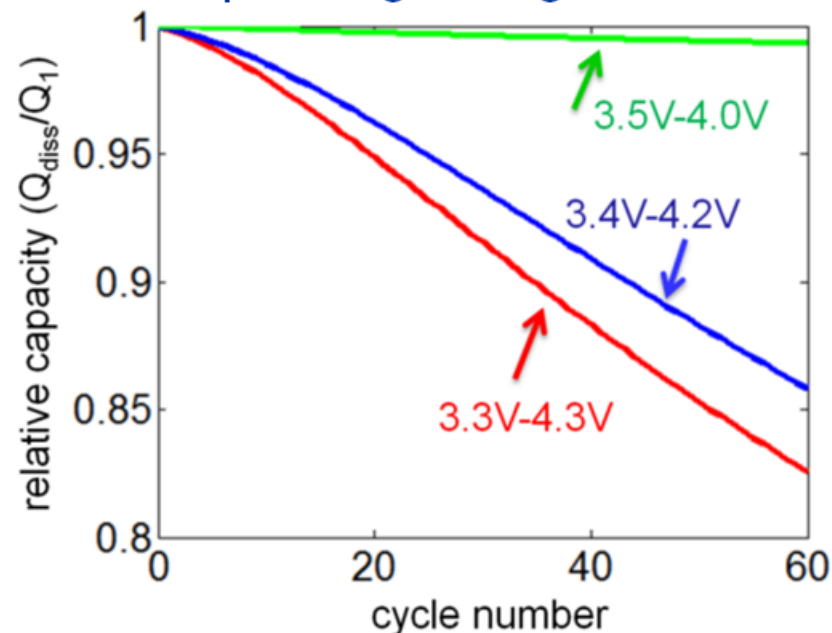


# dissolution of active particles: FY10 A • M • S • L

temperature effect



operating voltage effect



- due to a higher temperature and a wider range of voltages, greater dissolution of cathode particles was shown to result in a severe capacity fade using the models derived here
- the capacity fade increases by a factor of 5 when the temperature increases by 30 C after 60 cycles, and the cycling with a wider voltage range results in a 25% increase in the capacity fade after 60 cycles



## heat generation model [1,2]

- heat generation due to side reactions can be significant when thermal runaway starts
- heat of mixing  $O(10^{-14})$  is negligible compared to resistive heat  $O(10^{-12})$  and entropic heat  $O(10^{-12})$  at particle scale [2]

symbol	meaning
$T$	temperature
$\dot{Q}_g$	heat generation rate
$I$	current
$U$	open circuit potential
$V$	potential
$\Delta H_k^{\text{avg}}$	enthalpy of reaction for chemical reaction k
$r_k$	rate of reaction k
$\bar{H}_{ij}$	partial molar enthalpy of species i in phase j
$\bar{H}_{ij}^{\text{avg}}$	volume-averaged partial molar enthalpy
$c_{ij}$	concentration of species i in phase j

$$\dot{Q}_g = \underbrace{I_1 \cdot \nabla V_1 + I_2 \cdot \nabla V_2}_{\text{resistive heating}} + \underbrace{J(V_1 - V_2 - U)}_{\text{reaction heating}} + \underbrace{T \frac{\partial U}{\partial T}}_{\substack{\text{entropic heat} \\ \text{(reversible, due to} \\ \text{entropy change)} \\ \text{not considered}}} + \underbrace{\sum_k \Delta H_k^{\text{avg}} r_k}_{\text{heat change due to side reactions}} + \underbrace{\int \sum_j \sum_i (\bar{H}_{ij} - \bar{H}_{ij}^{\text{avg}}) \frac{\partial c_{ij}}{\partial t} dv}_{\text{heat of mixing (due to concentration gradient)}}$$

[1] Thomas, K.E. and Newman, J., "Thermal modeling of porous insertion electrodes," *J. Electrochem. Soc.*, v. 150, pp. A176-A192, 2003

[2] Zhang, X.C., Sastry, A.M., and W. Shyy, "Intercalation-induced stress and heat generation within single lithium-ion battery cathode," *J. Electrochem. Soc.*, v. 155(7), pp.A542-A552.



## microscopic scale

### 3-D electrode microstructure

liquid phase  
(electrolyte)



solid phase  
(active material)



both phase



interphase



$$\frac{\partial c_2}{\partial t} = \nabla \cdot (D_2 \nabla c_2)$$

$$\nabla \cdot [\kappa \nabla V_2 + \kappa_D \nabla (\ln c_2)] = 0$$

$$\frac{\partial c_1}{\partial t} = \nabla \cdot (D_1 \nabla c_1)$$

$$\nabla \cdot \mathbf{i}_1 = \nabla \cdot (\sigma \nabla V_1) = 0$$

$$\rho c_p \frac{\partial T_k}{\partial t} = \nabla \cdot (\lambda_k \nabla T_k) + \mathbf{i}_k \cdot \nabla V_k$$

Butler-Volmer equation

$$J = \frac{i_n}{F} = i_0 \left\{ \exp \left[ \frac{(1-\beta)F}{RT} \eta \right] - \exp \left[ -\frac{\beta F}{RT} \eta \right] \right\}$$

Arrhenius equation

$$\phi = \phi_{ref} \exp \left[ \frac{E_{act, \phi}}{R} \left( \frac{1}{T_{ref}} - \frac{1}{T} \right) \right]$$

volume  
averaging



## macroscopic scale

### 1-D Li-ion cell

anode | separator | cathode

$$\frac{\partial \bar{c}_2}{\partial t} = \nabla \cdot (D_2^{\text{eff}} \nabla \bar{c}_2) + J_{c_2}$$

$$\nabla \cdot [\kappa^{\text{eff}} \nabla \bar{V}_2 + \varepsilon_2 \kappa_D^{\text{eff}} \nabla (\ln \bar{c}_2)] + J_{V_2} = 0$$

$$\frac{\partial \bar{c}_1}{\partial t} = \nabla \cdot (D_1^{\text{eff}} \nabla \bar{c}_1) + J_{c_1}$$

$$\sigma^{\text{eff}} \nabla \bar{V}_1 + J_{V_1} = 0$$

$$\rho^{\text{eff}} c_p^{\text{eff}} \frac{\partial \bar{T}}{\partial t} = \nabla \cdot (\lambda^{\text{eff}} \nabla \bar{T}) + \bar{Q}$$

**closure terms ( $D^{\text{eff}}$ ,  $\kappa^{\text{eff}}$ ,  $\lambda^{\text{eff}}$ ,  $J$ ,  $Q$ ):**

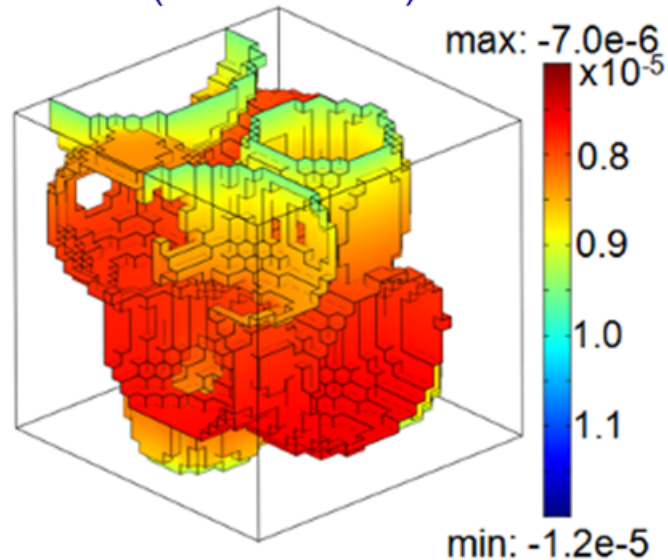
highly depend on the detailed microstructure

- effective material properties
- volumetric reaction current density
- heat generation

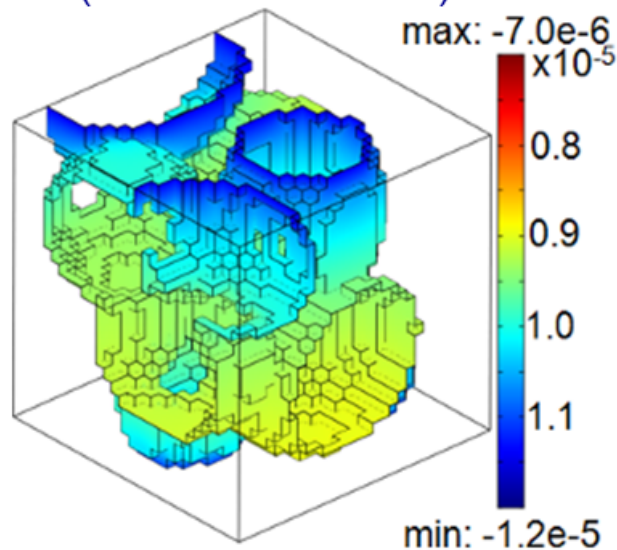


closure terms: reaction current density & heat generation at solid-electrolyte interphase (SEI)

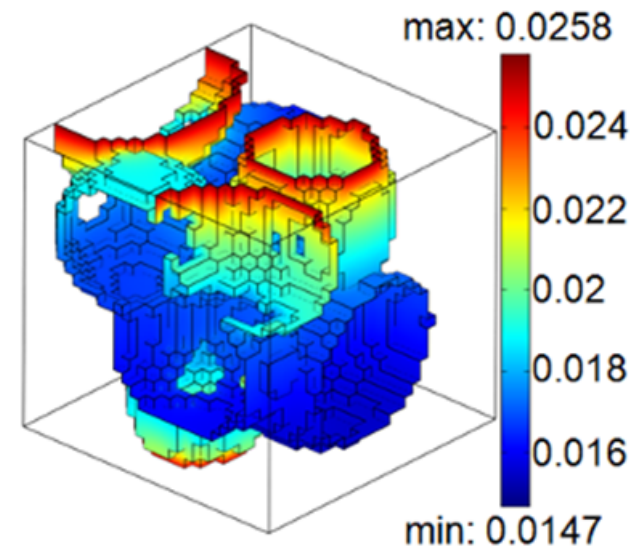
Li-ion flux  
(isothermal)



Li-ion flux  
(non-isothermal)



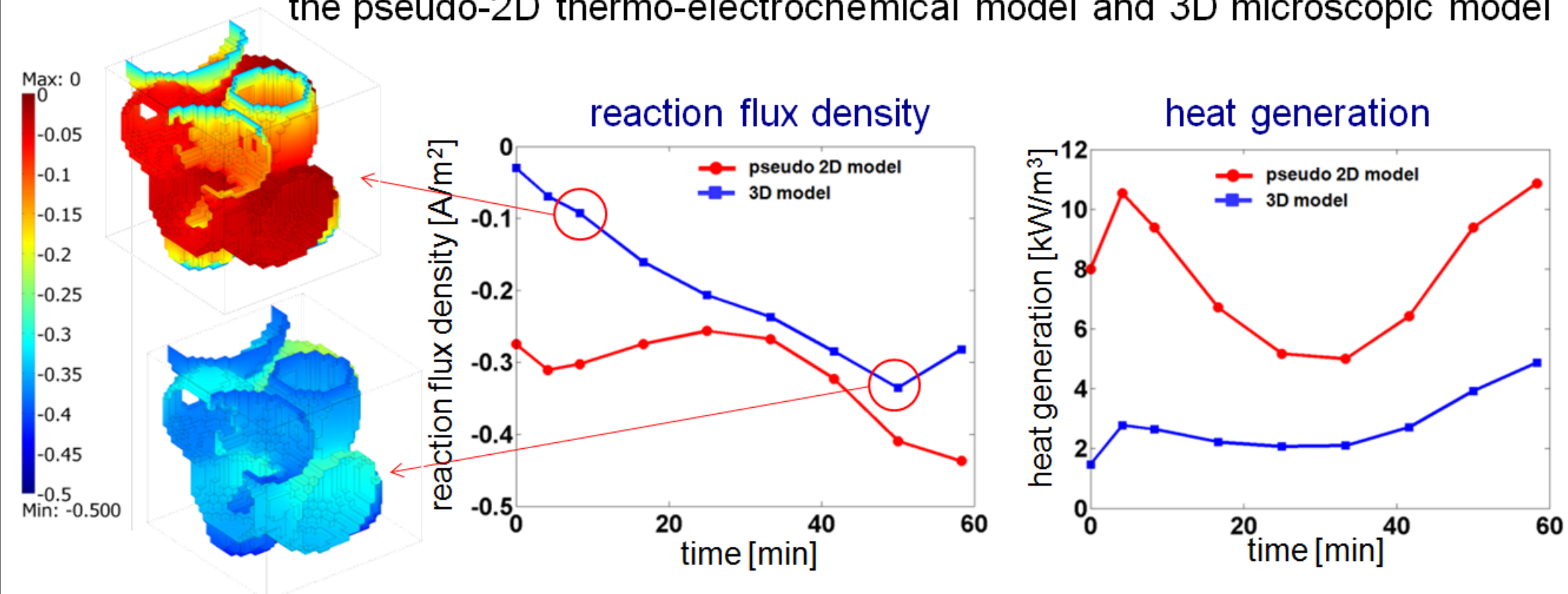
heat generation  
(non-isothermal)



non-isothermal model with temperature-dependent reaction and transport properties gives higher Li-ion flux at the solid-electrolyte interphase

## closure terms comparison

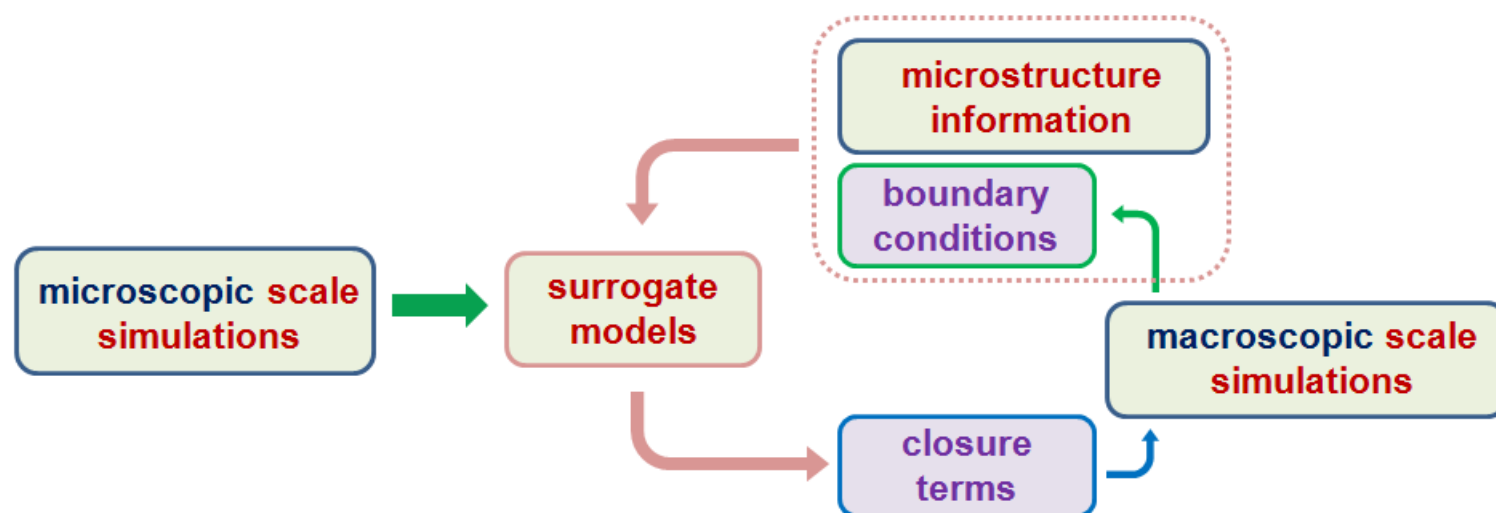
temporal variations of reaction current density and heat generation from the pseudo-2D thermo-electrochemical model and 3D microscopic model



3-D microscopic modeling of particle microstructure reveals distribution of local state variables (e.g., Li-ion concentration and electric potentials in solid and electrolyte phases)



## multiscale modeling: surrogate-based scale bridging



- surrogate modeling of closure terms (reaction current density and heat generation) in thermo-electrochemistry: key steps include design of experiment on state variables (e.g., Li-ion concentration and electric potentials), running numerical simulations, construction of surrogate models, validation
- global sensitivity analysis: constructed surrogate models are used to quantify quantification of the variation of the closure terms caused by state variables





## surrogate modeling of closure terms: reaction current density and heat generation

- design variables & their range

Variables	Symbol	Range	Unit
Li ion concentration (solid)	$\tilde{c}_1$	0.15 ~ 0.6	1
Li ion concentration gradient (solid)	$\tilde{c}_{1,z}$	-8000 ~ 1000	1/m
Electric potential (solid)	$V_1$	2.6 ~ 4.1	V
Electric potential gradient (solid)	$V_{1,z}$	-80 ~ 0	V/m
Li ion concentration (liquid)	$c_2$	800 ~ 2000	mol/m <sup>3</sup>
Li ion concentration gradient (liquid)	$c_{2,z}$	$-1.7 \times 10^7 \sim 6 \times 10^5$	mol/m <sup>4</sup>
Electric potential (liquid)	$V_2$	-1.5 ~ 0	V
Electric potential gradient (liquid)	$V_{2,z}$	-1300 ~ 0	V/m
Temperature	$T$	290 ~ 340	K
Temperature gradient	$T_z$	-1.5 ~ 0	K/m

- design space range

based on pseudo 2D solutions up to 3C discharge rates

- constraint of design space

bounds for surface overpotentials to avoid numerical issues from exponential term in Butler-Volmer equation

$$-0.1 \leq V_1 - V_2 - U(\tilde{c}_1) \leq 0$$

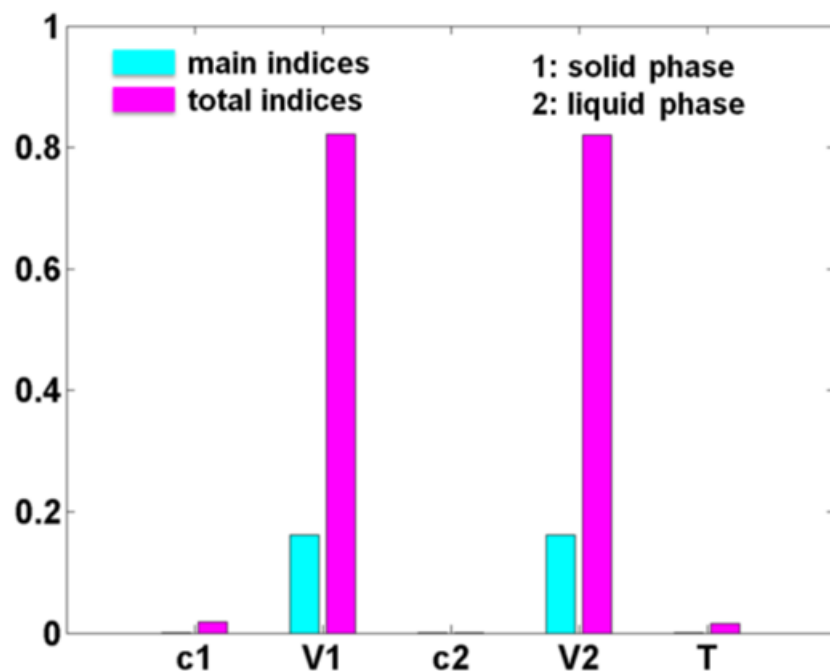
- design of experiments

face centered composite design (FCCD) and Latin hypercube sampling (LHS) were used to generate a set of simulation points as design of experiments (DOE).

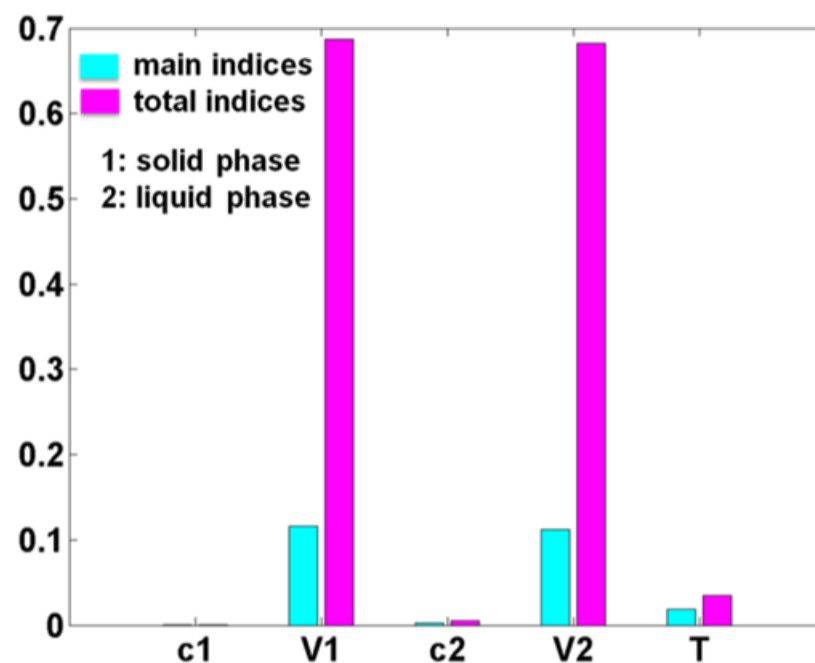


## global sensitivity analysis

reaction flux density



heat generation



electric potentials in solid and electrolyte phase dominates in surrogate models of reaction flux density and heat generation



# SEI formation modeling: FY10

A • M • S • L

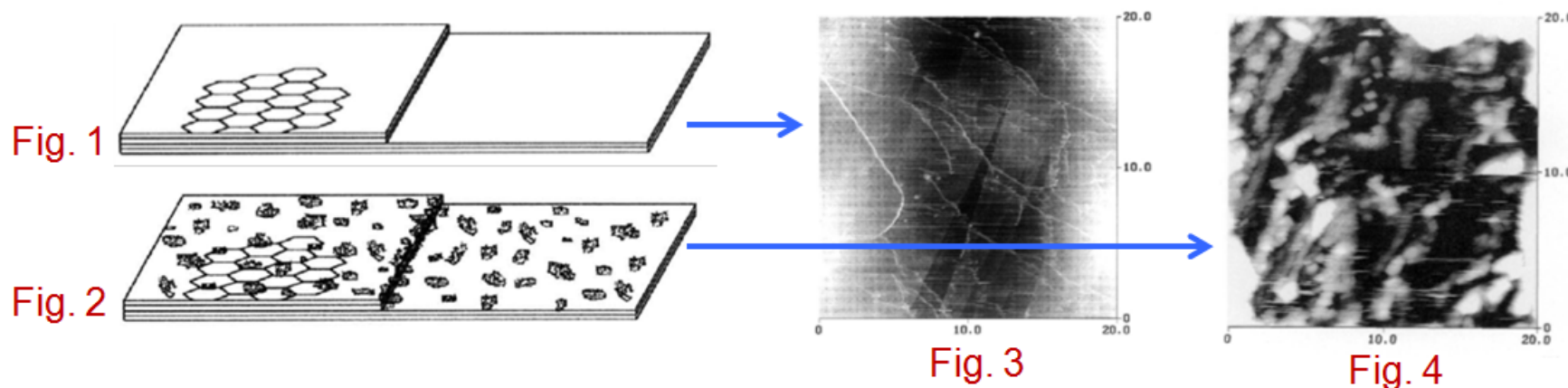
## experimental observation

### two distinct layers [1-4]

- a thin compact polycrystalline layer enriched with inorganic species (electrode side)
- a thick, porous, and amorphous layer enriched with organic compound (2<sup>nd</sup> layer)
- confirmed by XPS, SEM, AFM measurements

### nucleation and growth process [5]

- highly ordered pyrolytic graphite (HOPG) surface remains clean and smooth (higher than 2V, Fig 1,3); exhibit a few isolated solid islands on edge (below 1.6V); an abundance of solid clusters (below 0.8V, Fig 2,4)
- SEI is non-uniform and composed of secondary solid micrograins



[1] J. Yan *et al*, *Electrochimica Acta* 53, 7069 (2008)

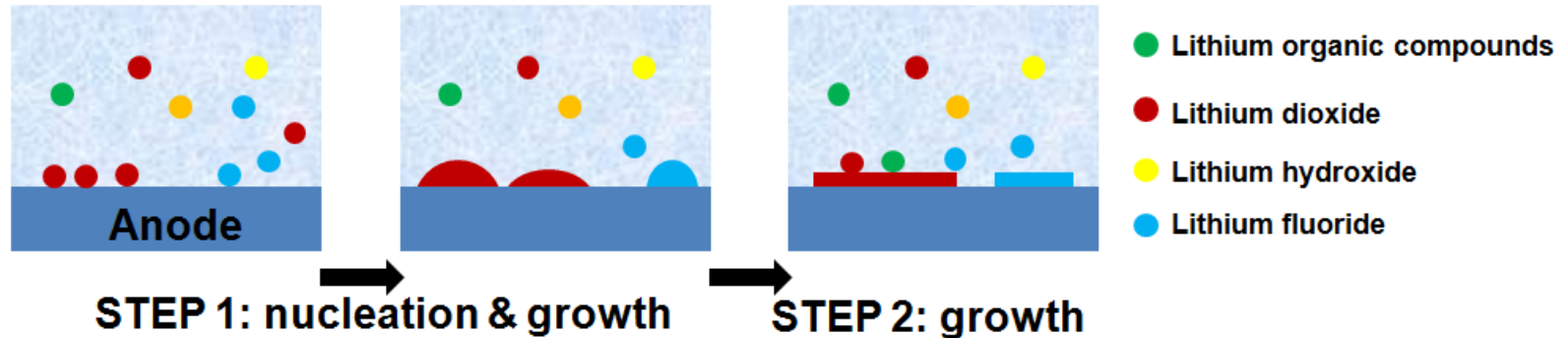
[2] D. Bar-Tow *et al*, *J. Electrochem. Soc.* 146, 824 (1999)

[3] A.M. Andersson *et al*, *J. Power Sources*, 119-121, 522 (2003)

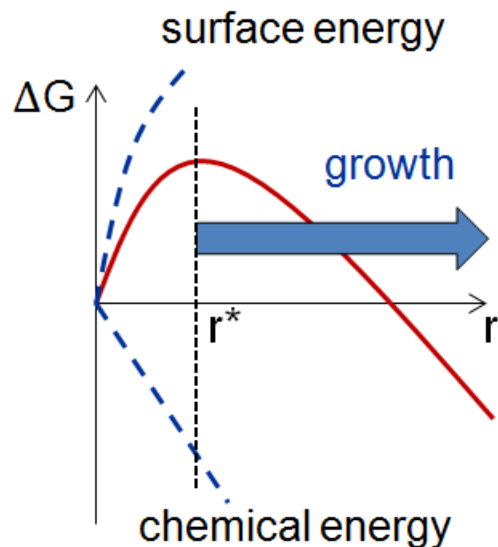
[4] D. Aurbach, *et al*, *J. Electrochem. Soc.* 143, 3525 (1996)

[5] A.C. Chu *et al*, *J. Electrochem. Soc.* 144, 4161 (1997)

## SEI formation



### nucleation [1,2]



- competition between chemical energy and surface energy
- some nuclei cannot grow, dissolve into the parent phase
- $r < r^*$ , surface energy dominates (shrinks)

- if a nucleation is formed, the final geometry affects the surface roughness, therefore the new-formed layer is affected by the pre-formed layers
- how to determine the geometry of the nucleation? microstructure evolution problem

[1] J. Yan et al, Electrochimica Acta, 53, 7069 (2008)

[2] J.W. Christian, The Theory of Transformations in Metals and Alloys, Oxford (2002)





# SEI formation modeling: FY10

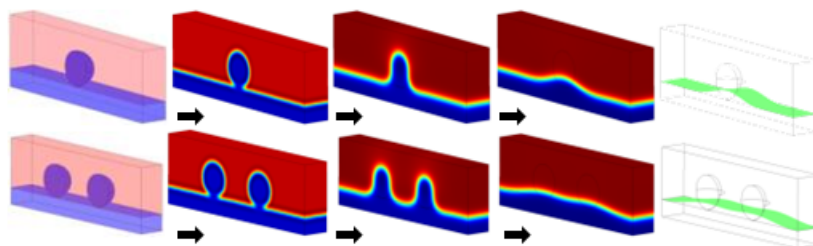
A • M • S • L

## phase field method approach

$$G = \int_{\Omega} \left( \underbrace{f(c)}_{\text{chemical energy}} + \underbrace{\frac{1}{2} h (\nabla c)^2}_{\text{interfacial energy}} \right) dS + \underbrace{\int_{\partial\Omega} [\sigma_{SA} + (\sigma_{SE} - \sigma_{SA}) \rho(c)] dl}_{\text{surface energy (S: solid, A: anode, E: electrolyte)}}$$

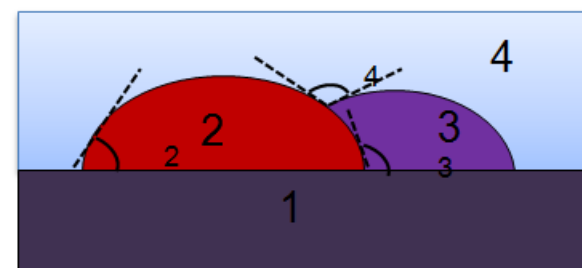
**extend (plan)**  
**roughness change**  
**(affect new layer)**

### single particle nucleation



$$\beta = L_c (\sigma_{SE} - \sigma_{SA}) / h$$

### hetero-nucleation

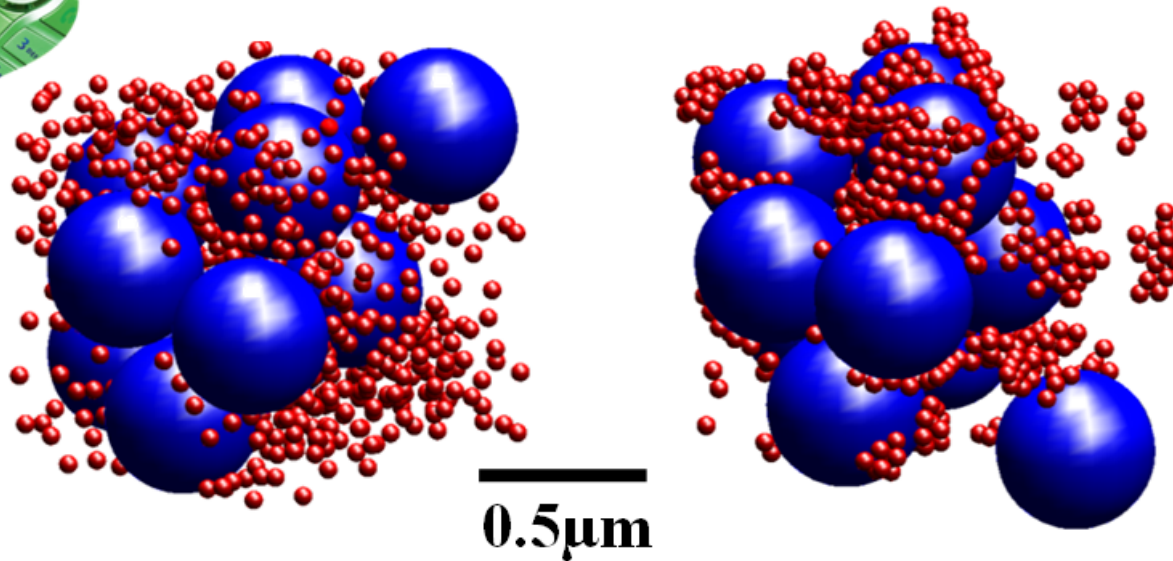


local equilibrium angles

$$\sigma_{14} - \sigma_{24} \cos \theta_2 - \sigma_{12} = 0$$

$$\sigma_{13} + \sigma_{12} - \sigma_{23} \cos \theta_3 = 0$$

$$\sigma_{13} - \sigma_{24} - \sigma_{34} \cos \theta_4 = 0$$



**initial configuration**

**final configuration**


**T=308K**

**active material particle  
size 0.5μm and 1.0μm**

**AM:CB mass ratio  
4%:92%**

**volume fraction of AM  
and CB: 50%**

**unit cell size: 4.7 times of  
the AM radius**

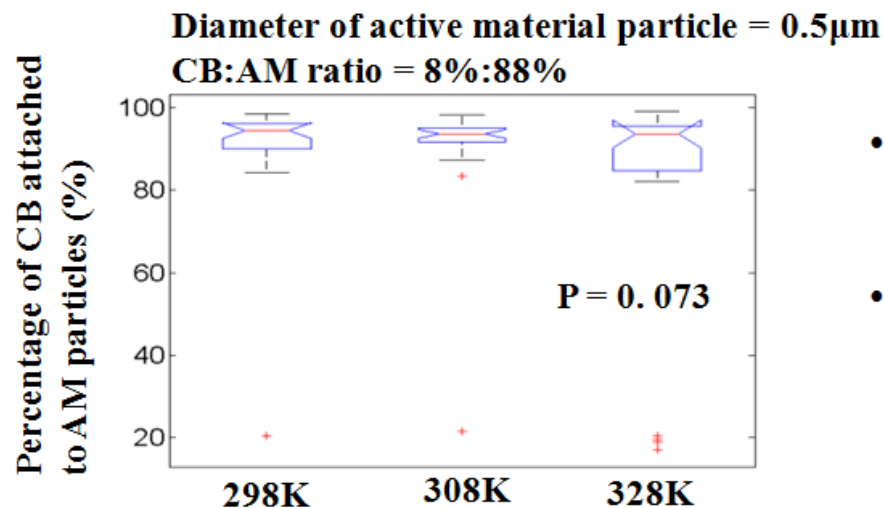
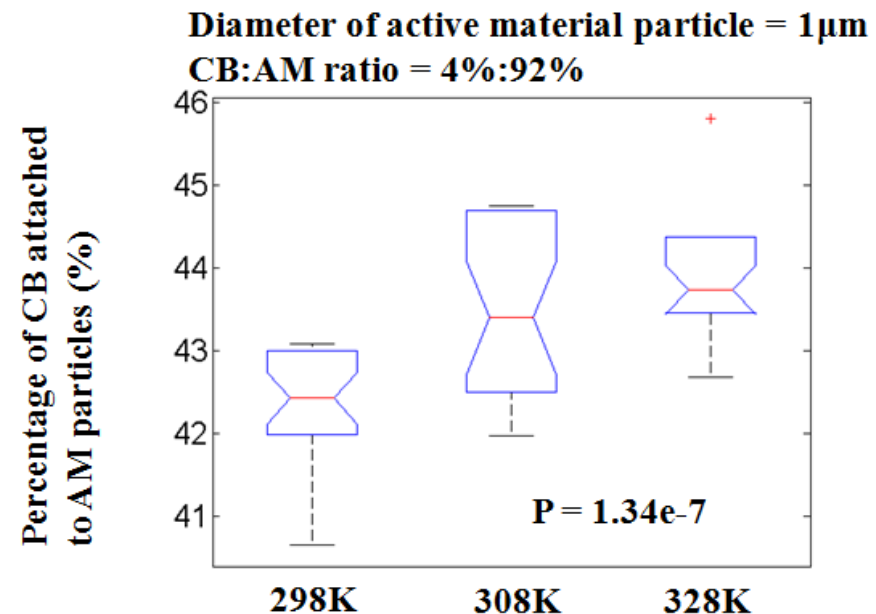
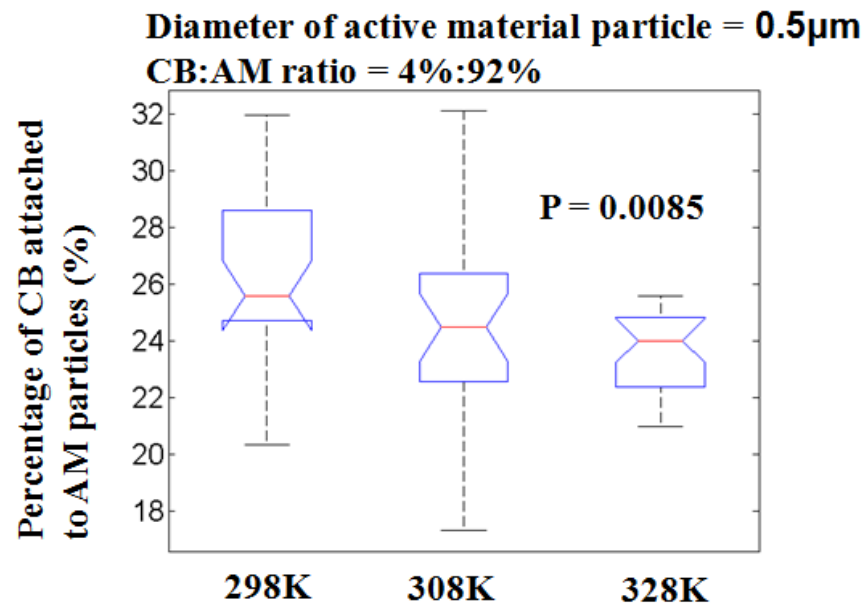
 **active material (AM)**  
 **carbon black (CB)**

- all AM particles are aggregated into a single cluster and percolate the simulation domain
- local aggregates of CB particles are observed
- CB particles are also observed to connect to the percolated AM clusters



# self-assembly in cathodes: FY10

A • M • S • L



- a larger AM particle size and larger CB/AM mass ratios each contribute positively to the percentage of CB attachment
- with increasing temperature this percentage increases in cases where AM particles have a diameter of  $1\mu\text{m}$  but decreases for AM particles whose diameter is  $0.5\mu\text{m}$



# accomplishments and status

A • M • S • L

- **Fundamental:** The changes in effective transport properties and electrochemical kinetics due to dissolution were incorporated into a thermo-electrochemical model to study capacity fade due to dissolution. **Practical:** this provides a quantitative and direct relationship between the volume fraction change due to dissolution and capacity fade.
- **Fundamental:** A multiscale thermo-electrochemistry was applied to include non-isothermal effects of the electrode microstructure on battery scale modeling. **Practical:** the constructed surrogate models give good predictions of the closure terms (i.e., reaction current density and heat generation) and reveal the significance of state variables (i.e., Li-ion concentrations and electric potentials).
- **Fundamental:** Brownian dynamics was employed to simulate the self-assembly of particles in Li-ion battery cathodes. **Practical:** the self-assembled structures were characterized by the percentage attachment of carbon black to active material clusters. The effect of temperature, mass ratio and particle size was investigated.
- **Fundamental:** The formation and evolution of the SEI layer was modeled, which had been observed via several experiments. **Practical:** The model explains the possible mechanism for the origin of the two distinct layers comprising the SEI layer.





# future work

A • M • S • L

- continue to refine numerical models based on findings from simulated performance and experiments; parameters to be investigated include multi-phase particle structures, resistances in SEI films, and temperature dependence of material transport properties and film resistance
- investigate SEI formation in composite electrode microstructures and its effect on battery kinetics and thermo-electrochemical performance; both experimental and numerical tools will be employed
- continue to explore progressive capacity degradation in composite multi-phase electrodes in the context of multiple scales and multiphysics coupling electrochemical kinetics and thermal effects



# summary

A • M • S • L

- numerical modeling of dissolution shows a quantitative relationship between the volume fraction change due to active material dissolution and capacity fade
- material loss of active particles results in decreased effective transport properties in the solid phase, which in turn results in a reduction in electrochemical reaction rate, reducing capacity
- 3-D microscopic modeling of particle microstructure reveals local distribution of state variables (Li-ion concentration and electric potentials) in thermal-electrochemical model
- global sensitivity analysis of surrogate models shows that electric potentials in solid and electrolyte phase dominates in the closure terms (reaction flux density and heat generation)
- self assembly simulation shows that a larger AM particle size and larger CB/AM mass ratios each contribute positively to the percentage of CB attachment
- with increasing temperature this percentage increases in cases where AM particles have a diameter of  $1\mu\text{m}$  but decreases for AM particles whose diameter is  $0.5\mu\text{m}$